Applications of Irradiance Tensors to the Simulation of Non-Lambertian Phenomena

James Arvo

Program of Computer Graphics*
Cornell University

Abstract

We present new techniques for computing illumination from non-diffuse luminaires and scattering from non-diffuse surfaces. The methods are based on new closed-form expressions derived using a generalization of irradiance known as *irradiance tensors*. The elements of these tensors are *angular moments*, weighted integrals of the radiation field that are useful in simulating a variety of non-diffuse phenomena. Applications include the computation of irradiance due to directionally-varying area light sources, reflections from glossy surfaces, and transmission through glossy surfaces. The principles apply to any emission, reflection, or transmission distribution expressed as a polynomial over the unit sphere. We derive expressions for a simple but versatile subclass of these functions, called *axial moments*, and present complete algorithms their exact evaluation in polyhedral environments. The algorithms are demonstrated by simulating Phong-like emission and scattering effects.

CR Categories and Subject Descriptors: I.3.7 [Computer Graphics]: Three-Dimensional Graphics and Realism.

Additional Key Words and Phrases: angular moment, axial moment, directional luminaire, double-axis moment, glossy reflection, glossy transmission, irradiance tensor.

1 Introduction

Rendering algorithms are frequently quite limited in the surface reflectance functions and luminaires they can accommodate, particularly when they are based on purely deterministic methods. To a large extent, this limitation stems from the difficulty of computing multi-dimensional integrals associated with non-diffuse phenomena, such as reflections from surfaces with directional scattering. While numerous closed-form expressions exist for computing the radiative exchange among uniform Lambertian (diffuse) surfaces with simple geometries [7, 12, 17], these expressions rarely apply in more general settings. Currently, the only approaches capable of simulating non-diffuse phenomena are those based on Monte Carlo [6, 20, 25, 26], hierarchical subdivision [3], or numerical quadrature [5, 18].

*580 Engineering and Theory Center Building, Ithaca, New York 14853, http://www.graphics.cornell.edu

Currently, few methods exist for computing semi-coherent reflections of a scene in a nearly-specular or *glossy* surface. The earliest examples of glossy reflection in computer graphics are due to Amanatides [1] and Cook [6]. Amanatides used cone tracing to simulate glossy reflections for simple scene geometries and reflectance functions. Cook introduced a general Monte Carlo method for simulating such effects that was later extended to path tracing by Kajiya [8] and applied to realistic surfaces by Ward [25]. Wallace et al. [24] approximated Phong-like directional scattering by rendering through a narrow viewing aperture using a z-buffer. Aupperle et al. [3] devised the first general deterministic method using three-point transfers coupled with view-dependent hierarchical subdivision.

This paper offers the first analytic method for computing direct lighting effects involving area light sources and a wide range of surfaces from diffuse to highly directional: such effects include illumination from directional luminaires and view-dependent glossy reflection and transmission. The method greatly extends the repertoire of effects that can be computed in closed form.

The present work begins with a tensor representation of irradiance comprised of *angular moments*, or weighted integrals of radiance with respect to direction [14]. Methods based on angular moments have a long history in the field of radiative transfer [9, 19], but are applied here in a fundamentally different way. In classical radiative transfer problems only low-order moments are relevant since detailed surface reflections can generally be ignored [19]. For image synthesis, where surface reflection is paramount, high-order moments can be used to capture the appearance of a non-diffuse surface or the distribution of a directional luminaire.

The idea of using high-order angular moments is extremely general and applies to all emission and reflectance functions that are polynomials over the sphere. The specific algorithms that we present, however, address only a limited class of polynomial functions; essentially the Phong distributions [13]. This class of polynomials has a representation that is simply related to irradiance tensors, and this leads to convenient closed-form expressions in polyhedral environments. The expressions are not much more difficult to evaluate than Lamabert's formula for irradiance [12, 17]; however, this does entail finding the visible contours of luminaires when occlusions are present.

The remainder of the paper is organized as follows. Section 2 introduces basic definitions and motivates the concept of irradiance tensors, which is further developed in section 3. These tensors apply to a much larger class of functions than those explored in this paper. Using irradiance tensors, we derive expressions for *axial moments* in section 4; these are a simple but convenient form of moment with immediate applications. In section 5 we focus on polygonal luminaires and derive several closed-form expressions which are then applied to three related non-diffuse simulations in section 6.

2 Radiometric Concepts

In this section we introduce the fundamental radiometric concepts used in the following sections as well as several concepts that motivate the notion of irradiance tensors.

Let $f(\mathbf{r}, \mathbf{u})$ denote a monochromatic radiance function [watts/m^{2}sr] defined at all points $\mathbf{r} \in \mathbb{R}^3$ and directions $\mathbf{u} \in \mathcal{S}^2$, where $\mathcal{S}^2$ is the set of all unit vectors in $\mathbb{R}^3$. The function f completely specifies the radiation field at large scales for a single wavelength. For fixed $\mathbf{r} \in \mathbb{R}^3$, the function $f(\mathbf{r}, \cdot)$ is known as the *directional distribution function*[1] [15, p. 29]. The goals of this paper are simply to obtain a useful characterization of $f(\mathbf{r}, \cdot)$ and apply it to the simulation of various direct lighting effects.

Most radiometric quantities can be defined in terms of weighted integrals of radiance. We shall examine three such quantities that lead naturally to irradiance tensors. First, the *monochromatic radiation energy density* [15] at the point $\mathbf{r} \in \mathbb{R}^3$ is defined by

$$u(\mathbf{r}) \equiv \frac{1}{c} \int_{\mathcal{S}^2} f(\mathbf{r}, \mathbf{u}) \; d\sigma(\mathbf{u}), \tag{1}$$

where c is the speed of light in the medium and σ denotes the canonical measure on the sphere [4, p. 276]; that is, $\sigma(A)$ is the surface area of any measurable subset $A \subset \mathcal{S}^2$. The function $u(\mathbf{r})$ is then the radiant energy per unit volume at $\mathbf{r}$, with units [joules/m^3]. Similarly, the *vector irradiance* [15] at $\mathbf{r}$ is defined by the vector integral

$$\Phi(\mathbf{r}) \equiv \int_{\mathcal{S}^2} \mathbf{u} \, f(\mathbf{r}, \mathbf{u}) \; d\sigma(\mathbf{u}), \tag{2}$$

which has the units [watts/m^2]. The scalar quantity $\Phi(\mathbf{r}) \cdot \mathbf{v}$ is the net flux of radiant energy through a surface at $\mathbf{r}$ with normal $\mathbf{v}$ [15]. Finally, the *radiation pressure tensor* [14] at $\mathbf{r}$ is a symmetric 3×3 matrix defined by

$$\Psi(\mathbf{r}) \equiv \frac{1}{c} \int_{\mathcal{S}^2} \mathbf{u}\,\mathbf{u}^{\mathrm{T}} \, f(\mathbf{r}, \mathbf{u}) \; d\sigma(\mathbf{u}), \tag{3}$$

where $\mathbf{u}\mathbf{u}^{\mathrm{T}}$ denotes an outer product; this function has the units [joules/m^3]. The bilinear form $\mathbf{w}^{\mathrm{T}}\Psi(\mathbf{r})\mathbf{v}$ is the rate at which photon momentum in the direction $\mathbf{w}$ flows across a surface at $\mathbf{r}$ with normal $\mathbf{v}$. Thus, each of the above integrals has a distinct interpretation and provides different information about the radiance distribution function at the point $\mathbf{r}$.

Note that in equations (2) and (3), the integral is in effect distributed across the elements of the vector or matrix. In equation (2) each element of the vector is a weighted integral of $f(\mathbf{r}, \cdot)$ where the weighting functions are first-order monomials on the sphere; that is, the direction cosines x, y, and z where $(x, y, z) \equiv \mathbf{u} \in \mathcal{S}^2$. Similarly, in equation (3) the weighting functions are the second-order monomials, x^2, y^2, z^2, xy, xz, and yz. These scalar-valued integrals respectively correspond to first- and second-order angular moments of the radiance distribution function.

3 Irradiance Tensors

The ideas of the previous section can be extended to higher orders using the formalism of tensors. Aside from the constant $1/c$, all of the integrals described in section 2 are multilinear functionals of the form

$$\int_{\mathcal{S}^2} \mathbf{u} \otimes \cdots \otimes \mathbf{u} \; f(\mathbf{r}, \mathbf{u}) \; d\sigma(\mathbf{u}), \tag{4}$$

where $\otimes$ denotes a tensor product. In this view, radiation energy density, vector irradiance, and the radiation pressure tensor are tensors of order 0, 1, and 2 respectively, with equation (4) providing the natural extension to tensors of all higher orders. Given that f is a radiance function, this family of tensors generalizes the notion of vector irradiance, with each member possessing the units of irradiance [watts/m^2]. Consequently, these new expressions are called *irradiance tensors* [2]. Although high-order irradiance tensors lack direct physical interpretations [14, p. 5], they are nevertheless useful vehicles for integrating polynomial functions over the sphere, as we demonstrate in this paper.

In this work we restrict $f(\mathbf{r}, \cdot)$ to be piecewise constant or piecewise polynomial over the sphere. Angular moments of f then reduce to polynomials integrated over regions of the sphere. To concisely represent these integrals we introduce a simplified form of irradiance tensor given by

$$\mathbf{T}^n(A) \equiv \int_A \underbrace{\mathbf{u} \otimes \cdots \otimes \mathbf{u}}_{n \text{ factors}} \; d\sigma(\mathbf{u}), \tag{5}$$

where $A \subset \mathcal{S}^2$ and $n \geq 0$ is an integer. The integrand of such a tensor contains all monomials of the form $x^i y^j z^k$ where $(x, y, z) \in \mathcal{S}^2$, and $i + j + k = n$; thus, $\mathbf{T}^n(A)$ consists of nth-order monomials integrated over A.

In what follows, the region $A \subset \mathcal{S}^2$ will represent the spherical projection of a luminaire $P \subset \mathbb{R}^3$, which we denote by $\mathbf{\Pi}(P)$. Without loss of generality, we may assume that the sphere is centered at the origin, as shown in Figure 1a. The tensors $\mathbf{T}^n(A)$ allow us to perform several useful computations; for example, we may compute angular moments of the illumination due to uniform Lambertian luminaires, or irradiance due to directionally varying luminaires.

Irradiance tensors of all orders are defined by surface integrals, and in some cases may be reduced to one-dimensional integrals by means of the generalized Stokes' theorem [22]. The resulting boundary integrals can be evaluated analytically for certain patch geometries, such as polygons. The foregoing approach extends the classical derivation of Lambert's formula for irradiance [10, 21], yielding more complex boundary integrals in the case of higher-order tensors.

To express the fundamental formula for $\mathbf{T}^n(A)$, we require some special notation. To conveniently index tensors of all

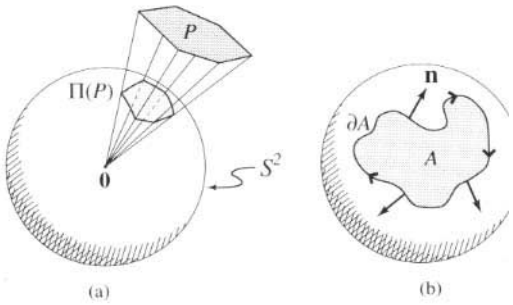

Figure 1: *(a) The surface P and its spherical projection $\mathbf{\Pi}(P)$ onto the unit sphere $\mathcal{S}^2$. (b) For any region $A \subset \mathcal{S}^2$, the unit vector $\mathbf{n}$ is normal to the boundary ∂A and tangent to the sphere.*

[1] Note that this function is distinct from a *radiant intensity distribution*, with the units of [watts/sr], which can be used to characterize a point light source.

orders, we shall use the n-index $\mathrm{I} \equiv (i_1, i_2, \ldots, i_n)$, where $i_k \in \{1, 2, 3\}$ for $1 \le k \le n$. We define I_k to be the kth sub-index, and I/k to be the $(n-1)$-index obtained by deleting the kth sub-index. That is,

$$\mathrm{I}/k \equiv (i_1, i_2, \ldots, i_{k-1}, i_{k+1}, \ldots, i_n).$$

Using this notation, we may concisely express the formula for irradiance tensors that will be our starting point. For all integers $n \ge 0$ and $A \subset \mathcal{S}^2$, the tensor $\mathbf{T}^n(A)$ satisfies the recurrence relation

$$\begin{aligned}(n+1)\ \mathbf{T}^n_{\mathrm{I}_j}(A) \ &= \ \sum_{k=1}^{n-1} \delta(\mathrm{I}_k, j)\ \mathbf{T}^{n-2}_{\mathrm{I}/k}(A) \\ &- \ \int_{\partial A} (\mathbf{u} \otimes \cdots \otimes \mathbf{u})_{\mathrm{I}}\, \mathbf{n}_j\, ds, \end{aligned} \qquad (6)$$

where I is an $(n-1)$-index, and Ij is the n-index formed by appending j to I. Here $\mathbf{n}$ denotes the outward normal to the boundary curve ∂A as shown in Figure 1b, ds denotes integration with respect to arclength, and $\delta(i, j)$ is the Kronecker delta, which is one if $i = j$ and zero otherwise.

Equation (6) follows from the generalized Stoke's theorem [2] and states that each tensor of the form defined in equation (5) can be reduced to a boundary integral and a term constructed from the tensor of two orders lower. The base cases $\mathbf{T}^{-1}(A) \equiv 0$ and $\mathbf{T}^0(A) \equiv \sigma(A)$ complete the recurrence relation.

It follows from equation (6) that $\mathbf{T}^n(A)$ can be computed analytically whenever the boundary integrals and base case can be. In particular, when A is the spherical projection of a k-sided polygon and $n = 1$, equation (6) yields

$$\mathbf{T}^1_j(A) \ = \ -\frac{1}{2}\int_{\partial A} \mathbf{n}_j\, ds \ = \ -\frac{1}{2}\sum_{i=1}^{k} \Theta_i\, \mathbf{n}^i_j, \qquad (7)$$

where Θ_i is the length of the arc corresponding to the ith edge of the polygon, and $\mathbf{n}^i$ is its outward normal. This is a well-known formula with numerous applications in computer graphics [12] originally derived by Lambert more than two centuries ago [17]. Although equation (6) is impractical computationally for moments of high order, it succinctly expresses the relationship among all the tensors. For instance, it is apparent that all even-order tensors incorporate solid angle $\mathbf{T}^0(A)$, while the odd-order tensors do not. We now derive several useful formulas from this equation.

4 Axial Moments

From equation (6) we may obtain expressions for individual moments or sums of moments without explicitly constructing the tensors. This is of great practical importance since the size of $\mathbf{T}^n(A)$ grows exponentially with n, yet only $\mathrm{O}(n^2)$ of its elements are distinct. We first consider the special case of moments about an axis, which defines a simple class of polynomials over the sphere. Given an arbitrary subset $A \subset \mathcal{S}^2$ and a unit vector $\mathbf{w}$, we define the nth *axial moment* of A about $\mathbf{w}$ by

$$\bar{\tau}^n(A, \mathbf{w}) \equiv \int_A (\mathbf{w} \cdot \mathbf{u})^n \ d\sigma(\mathbf{u}). \qquad (8)$$

As a cosine to a power, the polynomial weighting function within $\bar{\tau}^n$ is essentially a Phong distribution centered around

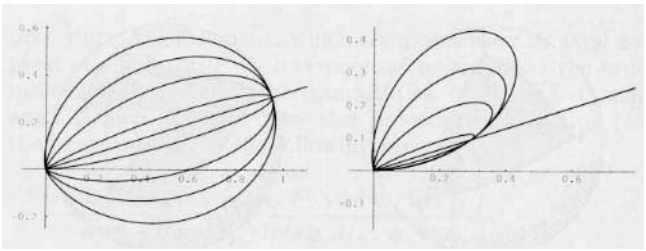

Figure 2: *Cross-sections of the weighting functions* $(\mathbf{w} \cdot \mathbf{u})^n$ *and* $(\mathbf{w} \cdot \mathbf{u})^n(\mathbf{v} \cdot \mathbf{u})$ *where* $\mathbf{v}$ *is the vertical axis; moment orders are 2, 4, 10, and 100, starting from the outer curves.*

the direction $\mathbf{w}$, as shown in Figure 2a. These functions are *steerable* in the sense that they can be re-oriented without raising their order [11]. The ease of controlling the shape and direction of the lobe makes this polynomial function useful in approximating reflectance functions, as Ward did with Gaussians [25], or an exact representation of simple Phong-like functions. To obtain a closed-form expression for $\bar{\tau}^n$, we begin by expressing the integrand of equation (8) as a composition of tensors:

$$(\mathbf{w} \cdot \mathbf{u})^n = (\mathbf{u} \otimes \cdots \otimes \mathbf{u})_{\mathrm{I}}\, (\mathbf{w} \otimes \cdots \otimes \mathbf{w})_{\mathrm{I}}. \qquad (9)$$

Here we have adopted the summation convention, where summation is implicit over all repeated pairs of indices; in equation (9) this means all sub-indices of I. It follows that

$$\bar{\tau}^n(A, \mathbf{w}) = \mathbf{T}^n_{\mathrm{I}}(A)(\mathbf{w} \otimes \cdots \otimes \mathbf{w})_{\mathrm{I}}, \qquad (10)$$

which associates the nth axial moment with the nth-order tensor. Using equation (6) to expand equation (10), and noting that $\delta(i, j)\mathbf{w}_i\mathbf{w}_j = \mathbf{w} \cdot \mathbf{w}$, we obtain

$$\begin{aligned}(n+1)\ \bar{\tau}^n \ &= \ (n-1)\ (\mathbf{w} \cdot \mathbf{w})\ \bar{\tau}^{n-2} \\ &- \ \int_{\partial A} (\mathbf{w} \cdot \mathbf{u})^{n-1}\ \mathbf{w} \cdot \mathbf{n}\ ds, \end{aligned} \qquad (11)$$

where the function arguments have been omitted for brevity. Equation (11) is a recurrence relation for $\bar{\tau}^n$ with base cases $\bar{\tau}^{-1}(A) = 0$ and $\bar{\tau}^0(A) = \sigma(A)$. When $n > 0$ the recurrence relation reduces to a single boundary integral involving a polynomial in $\mathbf{w} \cdot \mathbf{u}$. Since $\mathbf{w}$ is a unit vector, we have

$$\begin{aligned}(n+1)\ \bar{\tau}^n \ = \ \bar{\tau}^q \ - \ \int_{\partial A} \big[(\mathbf{w} \cdot \mathbf{u})^{n-1} + (\mathbf{w} \cdot \mathbf{u})^{n-3} + \cdots \\ + \ (\mathbf{w} \cdot \mathbf{u})^{q+1}\big]\ \mathbf{w} \cdot \mathbf{n}\ ds, \end{aligned} \qquad (12)$$

where $q = 0$ if n is even, and $q = -1$ if n is odd. This expression is useful as a component of more general expressions, such as double-axis moments.

4.1 Double-Axis Moments

An important generalization of equation (8) is to allow for moments with respect to multiple axes simultaneously; this will prove useful for handling radiant exchanges involving pairs of surfaces. We define the *double-axis moment* of A with respect to $\mathbf{w}$ and $\mathbf{v}$ by

$$\bar{\bar{\tau}}^{n,m}(A, \mathbf{w}, \mathbf{v}) \ \equiv \int_A (\mathbf{w} \cdot \mathbf{u})^n\ (\mathbf{v} \cdot \mathbf{u})^m\ d\sigma(\mathbf{u}). \qquad (13)$$

A recurrence relation for $\bar{\bar{\tau}}^{n,m}$ can also be obtained from equation (6) by expressing the integrand as a tensor composition with n copies of $\mathbf{w}$ and m copies of the vector $\mathbf{v}$. We

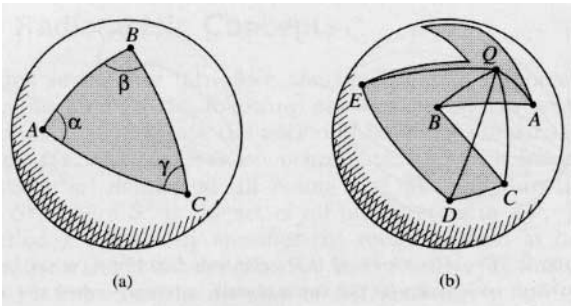

Figure 3: *(a) The solid angle of a spherical triangle is easily obtained from the internal angles. (b) Non-convex polygons can be handled by spoking into triangles from an arbitrary point Q.*

shall only consider the case where $m = 1$, which corresponds to $\mathbf{T}^{n+1}(A)(\mathbf{w} \otimes \cdots \otimes \mathbf{w} \otimes \mathbf{v})$ and yields the formula

$$\begin{aligned}(n+2)\ \bar{\bar{\tau}}^{n,1}(A, \mathbf{w}, \mathbf{v}) &= n\ (\mathbf{w} \cdot \mathbf{v})\ \bar{\tau}^{n-1}(A, \mathbf{w}) \\ &- \int_{\partial A} (\mathbf{w} \cdot \mathbf{u})^n\ \mathbf{v} \cdot \mathbf{n}\ ds. \end{aligned} \quad (14)$$

Figure 2a shows how an additional axis can change the shape of the weighting function. Note that when $\mathbf{v} = \mathbf{w}$, equation (14) reduces to the $(n+1)$-order axial moment given by equation (11). Recurrence relations for $\bar{\bar{\tau}}^{n,m}$ with $m > 1$ can be obtained in a similar manner, although the resulting boundary integrals are more difficult to evaluate.

Evaluating equations (12) and (14) in closed form is the topic of the next section. In section 6 we show how these moments apply to non-diffuse phenomena.

5 Exact Evaluation

Equations (6) and (12) reduce tensors and moments to one-dimensional integrals and (in the case of even orders) solid angle. This section describes how both of these components can be evaluated in closed form. Thus far no restrictions have been placed on the region $A \subset \mathcal{S}^2$; however, we shall now assume that A is the spherical projection of a polygon $P \subset \mathbb{R}^3$, which may be non-convex. The resulting projection is a *geodesic* or *spherical* polygon, whose edges are great arcs; that is, segments of great circles.

When P is a polygon, the computation of solid angles and boundary integrals are both greatly simplified. Because the outward normal $\mathbf{n}$ is constant along each edge of a spherical polygon, the factors of $\mathbf{w} \cdot \mathbf{n}$ and $\mathbf{v} \cdot \mathbf{n}$ can be moved outside the integrals in equations (12) and (14) respectively. A second simplification emerges in parametrizing the boundary integrals, as shown below.

5.1 Solid Angle

The surface integral defining the solid angle subtended by P does not reduced to a boundary integral; this is because the corresponding differential 2-form is not exact [22, p. 131]. Fortunately, the solid angle subtended by a polygon can be computed directly in another way. If P is a triangle in $\mathbb{R}^3$ its projection $\mathbf{\Pi}(P)$ is a spherical triangle $\triangle ABC$. Girard's formula for spherical triangles [4, p. 278] states that

$$\sigma(\triangle ABC) = \alpha + \beta + \gamma - \pi, \quad (15)$$

where α, β, and γ are the three internal angles, as shown in Figure 3a. The internal angles are the dihedral angles between the planes containing the edges. For instance, the angle α in Figure 3a is given by

$$\alpha = \cos^{-1} \frac{(B \times A) \cdot (A \times C)}{\| B \times A \| \| A \times C \|}. \quad (16)$$

Equation (15) generalizes immediately to arbitrary convex polygons [4, p. 279]. One way to compute the solid angle subtended by an arbitrary polygon is to cover its spherical projection with n triangles, all sharing an arbitrary vertex $Q \in \mathcal{S}^2$. See Figure 3b. The solid angle is then the sum of the triangle areas signed according to orientation. In the figure, $\triangle QAB$, $\triangle QCD$, and $\triangle QDE$ are all positive, while $\triangle QBC$ is negative, according to the clock-sense of the vertices. This method does not require $\mathbf{\Pi}(P)$ to be decomposed into triangles.

5.2 Boundary Integrals

The boundary integrals in equations (12) and (14) can be approximated by numerical quadrature, or evaluated analytically in terms of $\mathrm{O}(n)$ elementary functions per edge. We shall only describe analytic evaluation and a related approximation, both based upon a sum of integrals of the form

$$F_n(x, y) \equiv \int_x^y \cos^n \theta\ d\theta. \quad (17)$$

These integrals may be evaluated exactly using a recurrence relation given below. To express the integral in equation (12) in terms of $F_n(x, y)$ when A is a spherical polygon, we parametrize the great arc corresponding to each edge by

$$\mathbf{u}(\theta) = \mathbf{s} \cos\theta + \mathbf{t} \sin\theta,$$

where $\mathbf{s}$ and $\mathbf{t}$ are orthonormal vectors in the plane of the edge, with $\mathbf{s}$ directed toward the first vertex. To simplify the line integral over a great arc $\zeta \subset \mathcal{S}^2$, let ℓ be the length of the arc, and let $a \equiv \mathbf{w} \cdot \mathbf{s}$, $b \equiv \mathbf{w} \cdot \mathbf{t}$, and $c \equiv \sqrt{a^2 + b^2}$. Then by the above parametrization, we have

$$\begin{aligned}\int_\zeta (\mathbf{w} \cdot \mathbf{u})^n ds &= \int_0^\ell [\, a \cos\theta + b \sin\theta \,]^n\ d\theta \\ &= c^n \int_0^\ell \cos^n(\theta - \phi)\ d\theta, \\ &= c^n\, F_n(-\phi, \ell - \phi), \end{aligned} \quad (18)$$

where ϕ is the angle satisfying $\cos\phi = a/c$ and $\sin\phi = b/c$. To evaluate equation (18), we integrate equation (17) by parts to obtain the recurrence relation

$$\begin{aligned}F_n(x, y) = \frac{1}{n} \Big[&\cos^{n-1} y \sin y - \cos^{n-1} x \sin x \\ &+ (n-1)\, F_{n-2}(x, y) \Big], \end{aligned} \quad (19)$$

where $F_0(x, y) = y - x$ and $F_1(x, y) = \sin y - \sin x$. By means of this recurrence relation the function $F_n(x, y)$ may be evaluated in $\lfloor (n+1)/2 \rfloor$ steps. The complete integral in equation (12) is a weighted sum of these integrals for a sequence of different exponents, which are all even or all odd. The corresponding sequence of integrals can be computed incrementally, as demonstrated in the following section.

5.3 Algorithms for Efficient Evaluation

We now show that nth-order axial moments of k-sided polygons may be computed exactly (in the absence of roundoff error) in $O(nk)$ time. The algorithm evaluates equation (12) in $O(n)$ time for each of the k edges, using recurrence relation (19). The steps are broken into three procedures: *CosSumIntegral*, *LineIntegral*, and *BoundaryIntegral*. The first of these is the key to efficient evaluation; procedure *CosSumIntegral* computes the sum

$$c^k F_k(x,y) + c^{k+2} F_{k+2}(x,y) + \cdots + c^n F_n(x,y), \qquad (20)$$

where $k = m$ if $m + n$ is even, and $k = m + 1$ otherwise, for a given integer $m \geq 0$. The parameter m is included to accommodate both single- and double-axis moments. Because recurrence relation (19) generates integrals of cosine with increasing powers, all integrals in expression (20) may be generated as easily as the last term $c^n F_n(x,y)$. This strategy is embodied in the following procedure.

CosSumIntegral(**real** x, y, c; **int** m, n)
  $i \leftarrow$ **if even**(n) **then** 0 **else** 1;
  $F \leftarrow$ **if even**(n) **then** $y - x$ **else** $\sin y - \sin x$;
  $S \leftarrow 0$;
  while $i \leq n$ **do**
    if $i \geq m$ **then** $S \leftarrow S + c^i * F$;
    $T \leftarrow \cos^{i+1} y * \sin y \; - \; \cos^{i+1} x * \sin x$;
    $F \leftarrow [\, T + (i+1) * F \,] \,/\, (i+2)$;
    $i \leftarrow i + 2$;
    endwhile
  return S;
  end

The next procedure computes the line integral corresponding to a polygon edge; the steps correspond to equation (18), summed over a sequence of exponents from m to n.

LineIntegral(**vec** $\mathbf{A}, \mathbf{B}, \mathbf{w}$; **int** m, n)
  if $(n < 0)$ **or** $(\mathbf{w} \perp \mathbf{A}$ **and** $\mathbf{w} \perp \mathbf{B})$ **then return** 0;
  $\mathbf{s} \leftarrow$ *Normalize* $[\, \mathbf{A} \,]$;
  $\mathbf{t} \leftarrow$ *Normalize* $[\, (\mathbf{I} - \mathbf{s}\mathbf{s}^{\mathrm{T}})\, \mathbf{B} \,]$;
  $a \leftarrow \mathbf{w} \cdot \mathbf{s}$;
  $b \leftarrow \mathbf{w} \cdot \mathbf{t}$;
  $c \leftarrow \sqrt{a^2 + b^2}$;
  $\ell \leftarrow$ angle between $\mathbf{A}$ and $\mathbf{B}$;
  $\phi \leftarrow \mathrm{sign}(\, b \,) * \cos^{-1}(a/c)$;
  return *CosSumIntegral*$(-\phi, \ell - \phi, c, m, n)$;
  end

The next procedure, *BoundaryIntegral*, computes the complete boundary integral for a given k-sided polygon P by forming a weighted sum of k line integrals. The weight associated with each edge is the cosine of the angle between its outward normal and the second vector $\mathbf{v}$, which may coincide with $\mathbf{w}$.

BoundaryIntegral(**pgon** P; **vec** $\mathbf{w}$, $\mathbf{v}$; **int** m, n)
  $b \leftarrow 0$;
  for each edge **AB in** P **do**
    $\mathbf{n} \leftarrow$ *Normalize* $[\, \mathbf{A} \times \mathbf{B} \,]$;
    $b \leftarrow b + (\mathbf{n} \cdot \mathbf{v}) * \mathit{LineIntegral}(\mathbf{A}, \mathbf{B}, \mathbf{w}, m, n)$;
    endfor
  return b;
  end

With these three basic procedures we may now define the procedure *AxialMoment*, which computes the nth axial moment of a polygon P with respect to the axis $\mathbf{w}$. Even-order moments also require the computation of a "signed" solid angle, which is handled by this procedure. Equation (12) then corresponds to the following function.

AxialMoment(**pgon** P; **vec** $\mathbf{w}$; **int** n)
  $a \leftarrow -\mathit{BoundaryIntegral}(P, \mathbf{w}, \mathbf{w}, 0, n-1)$;
  if even(n) **then** $a \leftarrow a + \mathit{SolidAngle}(P)$;
  return $a \,/\, (n+1)$;
  end

The function *SolidAngle* returns the solid angle subtended by the polygon P using the method described in section 5.1. Because the sign of the boundary integral depends on the orientation of the polygon, the solid angle must be similarly signed. Thus, *SolidAngle* is positive if ∂P is oriented counter-clockwise as seen from the origin, and negative otherwise.

Finally, the procedure *DoubleAxisMoment* computes the nth-order moment of a polygon P with respect to the $\mathbf{w}$ axis and the 1st-order moment with respect to the $\mathbf{v}$ axis. Equation (14) then corresponds to the procedure

DoubleAxisMoment(**pgon** P; **vec** $\mathbf{w}, \mathbf{v}$; **int** n)
  if $n = 0$ **then return** *AxialMoment*$(P, \mathbf{v}, n)$;
  $a \leftarrow \mathit{AxialMoment}(P, \mathbf{w}, n-1)$;
  $b \leftarrow \mathit{BoundaryIntegral}(P, \mathbf{w}, \mathbf{v}, n, n)$;
  return $(n * a * \mathbf{w} \cdot \mathbf{v} \; - \; b) \,/\, (n+2)$;
  end

If we assume that trigonometric and other elementary functions are evaluated in constant time, then it is easy to see that procedures *AxialMoment* and *DoubleAxisMoment* both require $O(nk)$ time.

5.4 Optimizations

For clarity, the pseudo-code in the previous section does not depict a number of simple optimizations. For instance, the powers in procedure *CosSumIntegral* may be computed incrementally. Also, in computing double-axis moments, a great deal of redundant computation may be avoided by allowing procedure *CosSumIntegral* to return one additional term in the series. These optimizations do not change the time complexity of the algorithms, but can significantly reduce the constant.

Another means of speeding the computation is to settle for an approximation. Note that the terms in equation (12) decrease in magnitude monotonically because $|F_{k+2}| < |F_k|$ for all k, and $0 \leq c \leq 1$. When the terms approach zero rapidly we may obtain an accurate approximation with little work. Moreover, by bounding the tail of the series it is possible to guarantee any given tolerance. For example, to compute a double-axis moment to a relative accuracy of ϵ, the loop in *CosSumIntegral* may be terminated immediately upon updating S if the condition

$$\left| \frac{(\mathbf{v} \cdot \mathbf{n})\; c^n\, F}{(\mathbf{u} \cdot \mathbf{v})(\mathbf{u} \cdot \mathbf{n})} \right| \; + \; \left| \frac{c^k\, F}{1 - c^2} \right| \; \leq \; \epsilon \; |S| \qquad (21)$$

is met. In this case the tail of the series and the final integral in equation (14) may be dropped. Early termination of the loop is particularly useful with high orders; however, the test is costly and therefore should not be performed at every iteration of the loop.

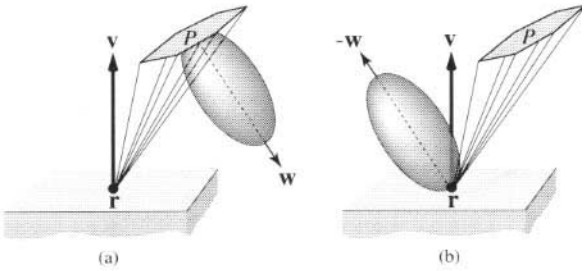

Figure 4: *(a) Computing the irradiance at the point* $\mathbf{r}$ *due to a directionally-varying area light source* P *is equivalent to (b) computing a double-axis moment of a uniform Lambertian source of the same shape.*

6 Applications

For ideal diffuse surfaces irradiance is sufficient to compute reflected radiance. The situation is dramatically different for non-diffuse surfaces, however. For surfaces that are neither ideal diffuse nor ideal specular, high-order moments can be used to quantify additional features of the incident illumination, in analogy with a power series expansion. For polygonal environments with emission and reflection distributions defined in terms of moments, the procedures given in the previous section may be used to simulate directional luminaires, glossy reflections, and glossy transmissions.

6.1 Directional Luminaires

Methods for simulating the illumination due to diffuse area sources [12] and directional point sources [23] are well known; however, directional area sources are problematic for deterministic algorithms. In this section we shall see how a class of directional luminaires can be handled using double-axis moments.

Let P be a polygonal luminaire whose emission distribution is spatially uniform but varies directionally according to a Phong distribution; that is, as a cosine to a power [13]. For instance, the direction of maximum radiance may be normal to the plane of the luminaire, falling off rapidly in other directions, as shown by the distribution in Figure 4a. The irradiance at the point $\mathbf{r}$ is then given by

$$\int_{\mathbf{\Pi}(P')} |\mathbf{u}\cdot\mathbf{w}|^n \cos\theta \; d\sigma(\mathbf{u}), \tag{22}$$

where P' is the visible portion of the luminaire P translated by $-\mathbf{r}$, and θ is the angle of incidence of $\mathbf{u}$; thus $\cos\theta = \mathbf{v}\cdot\mathbf{u}$, where $\mathbf{v}$ is the surface normal. Observe that this computation is equivalent to a double-axis moment of a Lambertian source P, where the nth moment is taken with respect to $-\mathbf{w}$ and the factor of $\cos\theta$ is accounted for by the second axis $\mathbf{v}$. See Figure 4b. Therefore, procedure *DoubleAxisMoment* can be used to compute the irradiance due to directional luminaires of this type in closed form.

Figure 5 shows a simple scene illuminated by an area source with three different directional distributions. Note that the areas directly beneath the luminaire get brighter with higher orders, while the surrounding areas get darker. Polygonal occlusions are handled by clipping the luminaire against all blockers and computing the contribution from each remaining portion, precisely as Nishita and Nakamae [12] handled Lambertian sources.

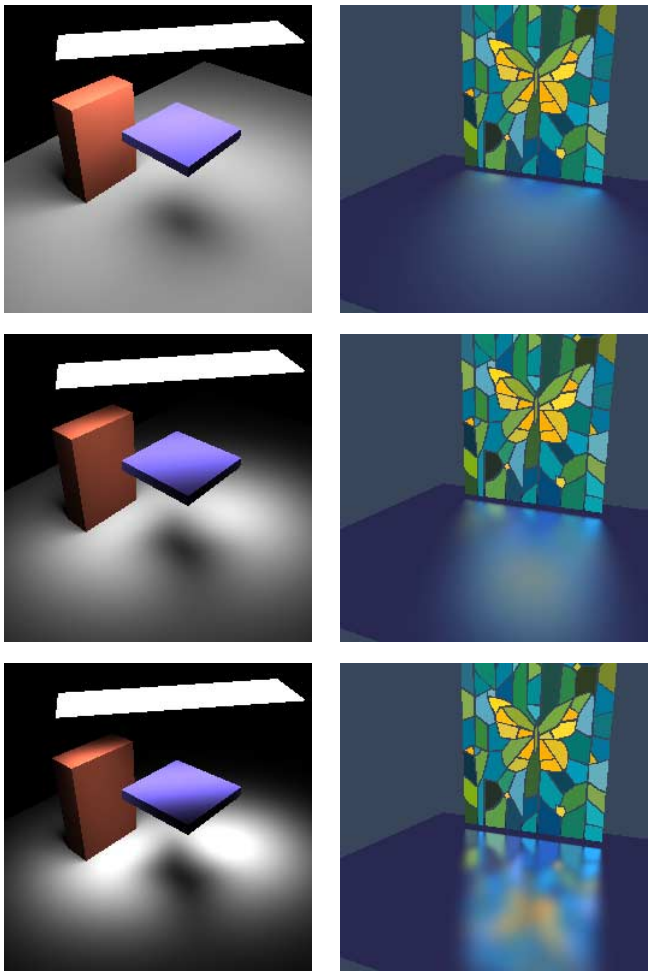

Figure 5: *(Left column) Irradiance from a directional luminaire computed analytically at each pixel; moment orders are 1, 10, and 20. (Right column) Analytic glossy reflection of a window design by Elsa Schmid [16]; moment orders are 10, 45, and 400.*

6.2 Glossy Reflection

A similar strategy can be used to compute glossy reflections of polygonal Lambertian luminaires. Let $\mathbf{r}$ be a point on a reflective surface. Then the reflected radiance at $\mathbf{r}$ in the direction $\mathbf{u}$ due to luminaire P is given by

$$f(\mathbf{r},\mathbf{u}) = \int_{\mathbf{\Pi}(P)} \rho(\mathbf{u}'\to\mathbf{u})\, f(\mathbf{r},\mathbf{u}') \cos\theta \; d\sigma(\mathbf{u}'), \tag{23}$$

where ρ is the bidirectional reflectance distribution function (BRDF) and θ is the angle of incidence of $\mathbf{u}'$. Now consider a simple BRDF defined in terms a Phong exponent. Let

$$\rho(\mathbf{u}'\to\mathbf{u}) \equiv c\, \left[\, \mathbf{u}^{\mathrm{T}} \left(\mathbf{I} - 2\mathbf{v}\mathbf{v}^{\mathrm{T}}\right) \mathbf{u}' \,\right]^n, \tag{24}$$

where c is a constant and $\mathbf{v}$ is the surface normal. Note that the Householder matrix $\mathbf{I} - 2\mathbf{v}\mathbf{v}^{\mathrm{T}}$ performs a reflection through the tangent plane at $\mathbf{r}$. This BRDF defines a cosine lobe about an axis in the direction of mirror reflection, as shown in Figure 6a. Because ρ obeys the reciprocity relation $\rho(\mathbf{u}'\to\mathbf{u}) = \rho(\mathbf{u}\to\mathbf{u}')$, the radiance reflected in the direction $-\mathbf{u}'$ is found by integrating over the distribution shown in the figure. To obey energy conservation the constant c must be bounded by $2\pi/(n+2)$.

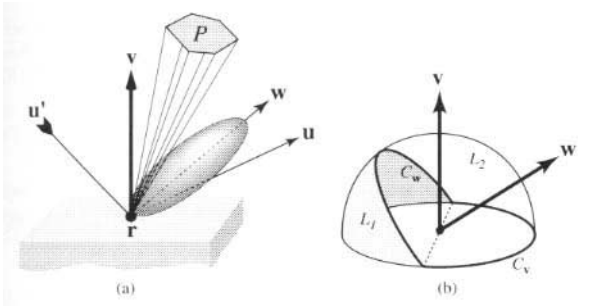

Figure 6: *(a) A simple BRDF defined by an axial moment around the mirror reflection* $\mathbf{w}$ *of* $\mathbf{u}'$*. By reciprocity, the radiance in the direction* $-\mathbf{u}'$ *due to* P *reduces to a double-axis moment of* P *with respect to* $\mathbf{w}$ *and* $\mathbf{v}$*. (b) The boundaries used for normalization.*

For a uniform Lambertian luminaire P, the function $f(\mathbf{r}, \cdot)$ is constant. In this case the integral in equation (23) reduces to a double-axis moment of P with respect to the vector

$$\mathbf{w} \equiv \left(\mathbf{I} - 2\mathbf{v}\mathbf{v}^{\mathrm{T}}\right)\mathbf{u}',$$

and the surface normal $\mathbf{v}$. Procedure *DoubleAxisMoment* may therefore be used in this context as well, to compute the glossy reflection of a diffuse luminaire. The technique is demonstrated in Figure 5 using a variety of moment orders to simulate surfaces with varying finishes.

More complex BRDFs may be formed by superposing lobes of different orders and/or different axes. Other effects such as anisotropic reflection and specular reflection near grazing can be simulated by allowing c and n to vary with the incident direction $\mathbf{u}'$; doing so does not alter the moment computations, however reciprocity is generally violated.

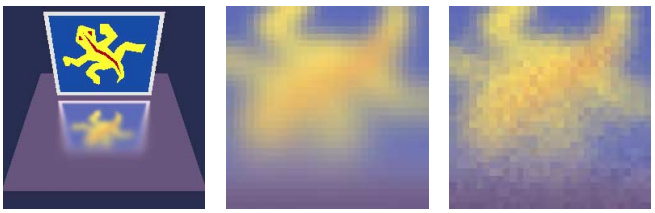

Figure 7: *A simple test scene with a glossy surface of order 300. The enlargemetns of the reflection were computed analytically (middle) and by Monte Carlo with 49 samples per pixel (right).*

In Figure 7 an exact solution is compared with a Monte Carlo estimate based on 49 samples per pixel; the samples were distributed according to the BRDF and stratified to reduce variance. Both methods operated directly on non-convex polygons in the scene. The run times were comparable: 6.5 seconds and 14.7 seconds respectively on an HP-755 workstation (100 MIPS). The analytic method eliminates the grainyness due to statistical noise and, in this instance, is also faster. The disparity in both time and quality is greater for lower moment orders and also for scenes with higher contrast.

6.3 Glossy Transmission

As a final example, we note that glossy transmission can be handled in much the same way as glossy reflection; the difference is in the choice of the axes $\mathbf{w}$ and $\mathbf{v}$, which must now exit from the far side of the transparent material. Figure 8 shows two images depicting "frosted glass", with different finishes

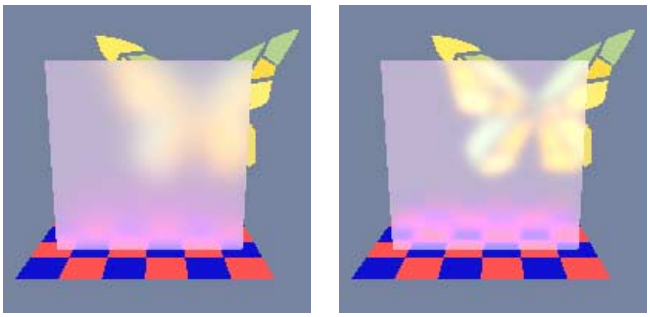

Figure 8: *A frosted glass simulation demonstrating glossy transmission. From left to right the moment orders are 10 and 65.*

corresponding to moments of different orders. This effect was first demonstrated by Wallace et al. [24] using a form of stochastic sampling; in Figure 8 a similar effect has been computed analytically using procedure *DoubleAxisMoment*.

6.4 Normalization

In applying the above methods, it is frequently useful to normalize the resulting distributions while ignoring negative lobes. We now show how this can be done for distributions defined in terms of double-axis moments.

The two planes orthogonal to the axes of a double-axis moment partition the sphere into four spherical *lunes* (also known as spherical *digons*); let L_1 and L_2 be the two lunes in the positive half-space defined by $\mathbf{v}$, as shown in Figure 6b. To normalize a BRDF, for example, we compute

$$N(\mathbf{w}, \mathbf{v}, n) \equiv \int_{L_2} (\mathbf{w} \cdot \mathbf{u})^n \, (\mathbf{v} \cdot \mathbf{u}) \; d\sigma(\mathbf{u}), \tag{25}$$

where $\mathbf{v}$ is the surface normal; thus, the integrand of equation (25) is positive for all exponents n on the lune L_2. Typically, luminaires must be clipped by the planes defining this lune before computing the moments.

Integral (25) can be evaluated analytically using equation (14), which results in two boundary integrals corresponding to the arcs $C_{\mathbf{w}}$ and $C_{\mathbf{v}}$. The special nature of the boundaries greatly simplifies the computation. For instance, $\mathbf{w} \cdot \mathbf{u}$ is zero on $C_{\mathbf{w}}$ while $\mathbf{v} \cdot \mathbf{n}$ is one on $C_{\mathbf{v}}$. Incorporating these facts, and accounting for the minor differences due to parity, we obtain a very simple means of evaluating integral (25) for arbitrary unit vectors $\mathbf{w}$ and $\mathbf{v}$, and any integer $n \geq 0$. The optimized code, which runs in O(n) time, is shown below.

```
N( vec w, v; int n )
    S ← 0;
    d ← w · v;
    c ← √(1 − d²);
    t ← if even(n) then π/2 else c;
    A ← if even(n) then π/2 else π − cos⁻¹ d;
    i ← if even(n) then 0 else 1;
    while i ≤ n − 2 do
        S ← S + T;
        T ← T * c² * (i + 1) / (i + 2);
        i ← i + 2;
        endwhile
    return 2 * (T + d * A + d² * S) / (n + 2);
    end
```

7 Conclusions

We have presented a number of new closed-form expressions for computing the illumination from luminaires with directional distributions as well as reflections from and transmissions through surfaces with a wide range of non-diffuse finishes. The expressions can be evaluated exactly in $O(nk)$ time for arbitrary non-convex polygons, where n is related to the directionality of the luminaire or glossiness of the surface, and k is the number of edges in the polygon.

To derive the new expressions we examined several well-known physical quantities as well as a tensor generalization of irradiance. Irradiance tensors satisfy a recurrence relation that subsumes Lambert's formula for irradiance and leads to expressions for *axial moments* and *double-axis moments*, which are quantities with direct applications in simulating non-diffuse phenomena. The resulting formulas give rise to easily implemented algorithms.

8 Future Work

An important extension of this work is to accommodate more realistic emission and reflectance distributions by expanding the class of polynomials over the sphere; these may be constructed by superposing cosine lobes, by introducing additional axes, or by forming linear combinations from some appropriate set of polynomial basis functions.

Useful extensions of equation (12) include non-integer orders and non-planar luminaires. Since equation (6) places no restriction on the boundaries, surfaces such as spheres also admit closed-form solutions; perhaps more general surfaces do as well. Equation (6) can be extended to handle luminaires with spatially varying distributions, although the resulting expressions involve special functions such as dilogarithms or Clausen integrals [2]. These expressions may prove useful in collocation-based methods for global illumination.

Axial moments of with three or more axes and arbitrary orders are a more immediate extension of the present work. With this type of moment it is possible to combine the effects demonstrated here; for example, glossy reflections of directional luminaires. Another application would be the simulation of non-diffuse surfaces illuminated by skylight using the polynomial approximation of a skylight distribution proposed by Nimroff et al. [11]. It can be shown that all moments of this form admit closed-form expressions, however efficient algorithms for their evaluation do not yet exist.

Acknowledgments

The author wishes to thank Peter Shirley for many valuable discussions, Albert Dicruttalo and Ben Trumbore for their assistance in modeling the stained glass window, and the anonymous reviewers for helpful comments. This research was supported by the NSF/ARPA Science and Technology Center for Computer Graphics and Scientific Visualization (ASC-8920219) and performed on workstations generously provided by the Hewlett-Packard Corporation.

References

[1] Amanatides, J. Ray tracing with cones. *Computer Graphics 18*, 3 (July 1984), 129–135.

[2] Arvo, J. *Analytic Methods for Simulated Light Transport*. PhD thesis, Yale University, 1995.

[3] Aupperle, L., and Hanrahan, P. A hierarchical illumination algorithm for surfaces with glossy reflection. In *Computer Graphics* Proceedings (1993), Annual Conference Series, ACM SIGGRAPH, pp. 155–162.

[4] Berger, M. *Geometry, Volume II*. Springer-Verlag, New York, 1987. Translated by M. Cole and S. Levy.

[5] Christensen, P. H., Stollnitz, E. J., Salesin, D. H., and DeRose, T. D. Wavelet radiance. In *Proceedings of the Fifth Eurographics Workshop on Rendering,* Darmstadt, Germany (1994), pp. 287–302.

[6] Cook, R. L. Distributed ray tracing. *Computer Graphics 18*, 3 (July 1984), 137–145.

[7] Howell, J. R. *A Catalog of Radiation Configuration Factors*. McGraw-Hill, New York, 1982.

[8] Kajiya, J. T. The rendering equation. *Computer Graphics 20*, 4 (August 1986), 143–150.

[9] Krook, M. On the solution of equations of transfer, I. *Astrophysical Journal 122*, 3 (November 1955), 488–497.

[10] Moon, P. *The Scientific Basis of Illuminating Engineering*. McGraw-Hill, New York, 1936.

[11] Nimroff, J. S., Simoncelli, E., and Dorsey, J. Efficient rerendering of naturally illuminated environments. In *Proceedings of the Fifth Eurographics Workshop on Rendering,* Darmstadt, Germany (1994), pp. 359–373.

[12] Nishita, T., and Nakamae, E. Continuous tone representation of 3-D objects taking account of shadows and interreflection. *Computer Graphics 19*, 3 (July 1985), 23–30.

[13] Phong, B. T. Illumination for computer generated pictures. *Communications of the ACM 18*, 6 (June 1975), 311–317.

[14] Pomraning, G. C. *The Equations of Radiation Hydrodynamics*. Pergamon Press, New York, 1973.

[15] Preisendorfer, R. W. *Radiative Transfer on Discrete Spaces*. Pergamon Press, New York, 1965.

[16] Schmid, E. *Beholding as in a Glass*. Herder and Herder, New York, 1969.

[17] Schröder, P., and Hanrahan, P. On the form factor between two polygons. In *Computer Graphics* Proceedings (1993), Annual Conference Series, ACM SIGGRAPH, pp. 163–164.

[18] Schröder, P., and Hanrahan, P. Wavelet methods for radiance computations. In *Proceedings of the Fifth Eurographics Workshop on Rendering,* Darmstadt, Germany (1994), pp. 303–311.

[19] Sherman, M. P. Moment methods in radiative transfer problems. *Journal of Quantitative Spectroscopy and Radiative Transfer 7*, 89–109 (1967).

[20] Shirley, P., and Wang, C. Distribution ray tracing: Theory and practice. In *Proceedings of the Third Eurographics Workshop on Rendering,* Bristol, United Kingdom (1992), pp. 33–43.

[21] Sparrow, E. M. A new and simpler formulation for radiative angle factors. *ASME Journal of Heat Transfer 85*, 2 (May 1963), 81–88.

[22] Spivak, M. *Calculus on Manifolds*. Benjamin/Cummings, Reading, Massachusetts, 1965.

[23] Verbeck, C. P., and Greenberg, D. P. A comprehensive light-source description for computer graphics. *IEEE Computer Graphics and Applications 4*, 7 (July 1984), 66–75.

[24] Wallace, J., Cohen, M. F., and Greenberg, D. P. A two-pass solution to the rendering equation: A synthesis of ray tracing and radiosity methods. *Computer Graphics 21*, 3 (July 1987), 311–320.

[25] Ward, G. J. Measuring and modeling anisotropic reflection. *Computer Graphics 26*, 2 (July 1992), 265–272.

[26] Ward, G. J. The RADIANCE lighting simulation and rendering system. In *Computer Graphics* Proceedings (1994), Annual Conference Series, ACM SIGGRAPH, pp. 459–472.